DEPARTMENT OF THE INTERIOR

U.S. GEOLOGICAL SURVEY

A Detailed Study of the Seismicity of the Middle Mountain Zone at Parkfield, California

Gail K. Nishioka

and

Andrew J. Michael [1]

September 21, 1989

OPEN-FILE REPORT 89-546

[1] Both at: U.S. Geological Survey
345 Middlefield Road - MS 977
Menlo Park, California 94025

ABSTRACT

A detailed study of the seismicity at Middle Mountain in the Parkfield, CA area was made using 71 earthquakes that located within, or close to, the Middle Mountain alert box. These earthquakes were retimed on the CUSP system. In an attempt to improve on the previous locations made using a velocity model derived from refraction data and the 1966 aftershock data (model O) and the station corrections derived by Poley (corrections P), two new sets of station corrections (sets 1 and 2) and one new velocity model (model N) were developed using a joint hypocentral location and velocity inversion program. The process of retiming the earthquakes and using the new station corrections (model O-1) reduced the rms traveltime residuals by 70% to 0.025 seconds, as compared to the standard catalog data located with model O-P. The velocity model N was determined by using the same layer boundaries as model O but allowed the velocities to change. Model N is similar to model O and with its set of station corrections (set 2) did not significantly reduce the rms traveltime residuals when compared with model O-1. Thus model O was accepted as a satisfactory velocity model for this region. The relocated seismicity in the Middle Mountain region is confined to a zone 1 1/2 kilometers wide. Cross sections looking toward 43° W of N revealed that the fault is dipping steeply, at 86°±1.1° NE. A 1 km. width of the fault zone is apparent in the northwest end of the study area. The 5° bend, as proposed by Lindh and Boore (1981), was detected in the first motion data but not in the hypocentral distribution. Fault plane solutions determined for the 71 earthquakes were mostly strike-slip or strike-slip within 90% confidence, the expected focal mechanism for the San Andreas fault. An event located in the north end of the study area co-locates with the strike-slip solutions and may be a thrust or oblique solution. Another earthquake, located 2 1/2 kilometers northeast of the fault, clearly has a thrust or north-south striking right lateral solution; either of which would indicate a component of fault-normal compression. The presence of these fault-normal compression events in the northern part of the study area could be related to a stress anomaly.

INTRODUCTION

This study examines the seismicity of the Middle Mountain area near Parkfield, California to determine the local seismogenic structure of the San Andreas fault. The structure of this expected nucleation zone for the predicted Parkfield characteristic earthquake (Bakun and McEvilly, 1984; Bakun and Lindh, 1985) is important to our understanding of the earthquake generation process. For example, Lindh and Boore (1981) suggested that the San Andreas fault bends 5° at this point. This fault bend may be related to fault segmentation (e.g. King and Nabalek, 1985). In addition Seeber and Armbruster (1988) state that the seismicity in the Parkfield region originates from two parallel faults and that almost half of the fault plane solutions can not be related to the San Andreas fault, but must come from secondary faults. As part of this study we will test these ideas with the higher quality data available starting in 1984, when the U.S.G.S. Northern California Seismic Network began digital recording. The quality of the data, together with the high station density that has resulted from the Parkfield Earthquake Prediction Experiment (Bakun and Lindh, 1985), allows us to also determine the width of the seismogenic zone and the fault plane solutions of small earthquakes with great accuracy.

Not only is it important to test the hypothesis from Lindh and Boore (1981) but, as we will show, it is not possible to do this with the results from other seismicity studies of the Parkfield area. McEvilly et al.'s (1967) analysis of the 1966 Parkfield aftershocks provides mostly epicenters and only a few focal depths. Eaton et al.'s (1970) study of the 1966 Parkfield aftershocks does not provide good locations of the earthquakes under Middle Mountain because their portable network was set up to study the cluster of aftershocks near Cholame Valley, at the other end of the Parkfield segment. Another problem with using the 1966 aftershock studies is that the area northwest of the epicenter was relatively quiet during the aftershock sequence, making it difficult to use that time period to study that part of the fault. However, during the background period since 1966 that part of the fault has been the most active area. Boore and Lindh (1981) did show earthquakes recorded during 1975, however while this is after the first major upgrade in the Parkfield part of the U.S.G.S. Northern California Seismic Network few details are given. Poley et al. (1987) give an interesting interpretation of the response of the Middle Mountain region to the 1983 Coalinga earthquake; however as will be shown their data set is not

adequate to address the fault bend hypothesis, nor did they attempt to address this question or the fault plane solutions. Seeber and Armbruster's (1988) analysis used only standard catalog phase data, as did both Poley et al. (1987), one of the major points of this paper is that this practice limits the scale at which one can work with the hypocentral locations and can provide erroneous fault plane solutions.

The San Andreas fault near Parkfield, California is the site of recurring, moderate-sized earthquakes with magnitudes of about 6 and a recurrence time of 22±5 years (Bakun and McEvilly, 1984). These earthquakes have similar magnitudes, locations, focal mechanisms, and rupture lengths. Instrumental records of the two most recent earthquakes, in 1934 and 1966, allowed Bakun and McEvilly (1984) to demonstrate that these events also had identical epicenters under Middle Mountain and unilateral ruptures to the southeast. The ruptures stopped near the offset in the fault trace southeast of Gold Hill (Lindh and Boore, 1981). The similarity of these recurring earthquakes suggest that this area of the San Andreas fault zone has earthquakes that repeat regularly and have predictable features (Bakun and McEvilly, 1984). The recurrence model for Parkfield earthquakes, proposed by Bakun and McEvilly (1984) and Bakun and Lindh (1985) resulted in a prediction for the next Parkfield earthquake. This study focuses on the recent seismicity near Middle Mountain, California, which is the expected hypocenter of the next Parkfield earthquake.

The San Andreas fault on which the Parkfield earthquakes have occurred, is the largest element of the transform plate boundary between the Pacific and North American plates. In Parkfield, the San Andreas fault zone divides the granitic, metamorphic and Cretaceous marine rocks of the Salinian block on the southwest from the complexly deformed Franciscan assemblage of the Diablo Range on the northeast (Dickinson, 1966). Previous geologic mapping (Dickinson, 1966; Dibblee, 1971a, 1971b, 1971c, 1971d) and more recent work by Sims (1988a, 1988b) indicate that the area surrounding the San Andreas in this region is transected by numerous thrust faults. Some of these are mapped within 1 km of the San Andreas and show Holocene displacements.

Careful retiming of the seismograms and relocation of the earthquakes combined with the determination of fault plane solutions should determine the seismogenic structure of the San Andreas fault and whether any of the other geologically mapped faults are seismically active. This analysis was

possible because of the high station density which yielded well-constrained locations and focal mechanisms for earthquakes with $M \geq 1.5$. This study also has a practical application to current attempts to make a short term prediction of the next Parkfield earthquake. The Middle Mountain alert box (Figure 1) is primary in the declaration of seismic alerts for the Parkfield region (Bakun et al., 1987) thus, mislocations of earthquakes in this area will affect the rate at which seismic alerts are declared for the Parkfield area under the Parkfield Earthquake Prediction experiment.

METHOD AND DATA

Data from U.S.G.S.-Calnet seismic stations were used in this study. Processing was done using the Caltech-U.S.G.S. Seismic Processing (CUSP) System where 480 channels are digitized at a rate of 100 Hz. Events were timed interactively on a CRT with a precision of 1/100th of a second. Routine timing for the catalog is done on a daily basis using the best P-wave arrivals at stations around the hypocenter. Parkfield earthquakes are then relocated using new station corrections developed by Poley et al. (1987) and the 1-D velocity model from Nowack, Ellsworth, and Lindh (unpublished data, 1982).

Fifty-seven earthquakes with $M \geq 1.5$ were selected from an area defined by the Middle Mountain alert box (Bakun et al., 1987) shown in Figure 1. This region is important for two reasons. Scientifically it is important to understand the structure of the expected hypocentral region of the next Parkfield earthquake. On a practical level the short-term alert criteria (Bakun et al., 1987) make it important to be confident of our ability to accurately locate events in this region. To augment these events, several others were chosen that were well recorded (greater than 20 stations read) even though they had $M < 1.5$. Outside of the Middle Mountain alert box, events located south of 36° 1′ N were included if their magnitudes were greater than 1.5 and they had 20 or more stations read. These events were just outside the box, but close enough that a slight (up to 1 kilometer) change in location could include the event within the limits of the box. A total of 71 well-recorded events were used in this study (Table 1). The events occur from April 1984, when digital recording on the CUSP system began, to the end of September 1987.

Once the data set was selected, it was processed in the following way. First, the entire data set

was retimed using the CUSP system. In this stage, the major differences introduced into the data set are the additions of new P arrival picks on stations that were not previously read, minor adjustment of arrival times on previously read stations, and rarely changes in first motion picks on previously read stations. The CUSP system allows the analyst to give a quality code to each arrival from 0 (best) to 3 (worst). Figure 2 shows examples of waveforms for each of these quality classes. After the data set was retimed it was analyzed with VELEST (Roecker and Ellsworth, 1978) a joint hypocentral and velocity inversion program. This technique simultaneously solves for new hypocenters, origin times, layer velocities, and station corrections. Next, using the new velocity model and station corrections, the events were relocated with HYPOINVERSE (Klein, 1985). One of the reasons for doing this is that HYPOINVERSE estimates the errors in the locations, while VELEST does not. Finally, first motion fault plane solutions were determined for each event using FPFIT (Reasenberg and Oppenheimer, 1985). FPFIT is a grid search program that estimates both the best focal mechanism and its confidence limits.

HYPOCENTRAL RELOCATIONS

Figure 3A shows the original locations as determined by Poley et al. (1987). These locations use the routine timing done by the CUSP group in order to develop the Northern California catalog, a velocity model developed by R. Nowack, W. Ellsworth, and A. Lindh using refraction and 1966 aftershock data (written communication, 1987; Figure 4), and station corrections developed by Poley et al. (1987). For future reference this model will be referred to as O-P for "O"ld Model and "P"oley et al.'s station corrections. Figure 3B shows the locations after retiming and using the same model: O-P. By retiming the events, the average rms traveltime residual was reduced from 0.083 to 0.062 seconds and there is a tighter clustering of events, especially of those to the south. Retiming the events is important because the time constraints of keeping the Northern California catalog current does not allow the analyst to spend much time on any individual earthquake. However, in a study such as this one, timing can be done more accurately because the data set is small and more time is spent on each event.

In order to further reduce the travel time residuals two new sets of station corrections and one new velocity model were developed using VELEST (Roecker and Ellsworth, 1978; modified by

Kissling, personal communication 1987). First new station corrections (set 1) were determined for use with velocity model O. The use of model O-1 reduced the average rms residual to 0.025 seconds. Only stations with an epicentral distance of less than 40 km are used to determine the hypocenters. On the average, 13 stations met this criteria for each event and were used in the locations. This step also shows better clustering of the seismicity than the initial relocations using model O-P. (Figure 5). If we assume the fault is planar, then the clustering of the earthquakes can be quantified by using the rms distances between the hypocenters and a reference plane (The reference plane is determined with a least-square fit of a plane to the hypocenters). For the Poley et al. (1987) locations the horizontal misfit is 0.40 km., while for those shown in Figure 5, the rms distance is only 0.21 km.

In an attempt to even further reduce the travel-time residuals, a second velocity model was developed (model N). For this model new station corrections (set 2) and new layer velocities were determined. The original and new velocity models are very similar (Figure 4) and relocating the earthquakes with model (N-2) only decreased the rms residual to 0.024 seconds. We choose the original starting model with the new station corrections (model O-1) as our final model because this small decrease in rms residual (0.001s) did not justify changing the velocity model and because model O was determined with refraction and earthquake data while the determination of model N used only earthquake data.

Events were then relocated with model O-1 using HYPOINVERSE (Klein, 1985). The final locations are shown in Figure 5, and listed in Table 1. Seismicity is confined to within 1 1/2 kilometers of the mapped trace of the San Andreas fault, except for one earthquake which locates 2 1/2 kilometers northeast of the trace of the fault at a depth of 13.42 kilometers. This earthquake will be discussed in more detail later. From the cross section taken along the fault (Figure 6) it is apparent that the seismicity deepens toward the center of the zone, as noted by Poley et al. (1987).

To test if the earthquakes occur on a simple planar structure, the cross section at B-B' (Figure 7) was taken perpendicular to the fault at an azimuth of 48° east of north. The azimuth of the cross-section was chosen to minimize the squared horizontal misfit between the hypocenters and the reference plane. The 95% confidence limits were determined by non-parametric bootstrap statistics (Efron and

Tibshirani, 1986). The best plane (Figure 7) dips at 86°±1.2°; the rms misfit of the events to this plane is 0.21 km. The events that locate at 10 to 14 kilometers depth are the ones that appear off the fault in map view due to the 86° dip of the fault. It is possible that the fault is actually vertical and that the 86° dip is an artifact of the plane-layered velocity model used.

While the events do appear to fall near a single plane, some structure is apparent. The fault zone appears to have a width of approximately 1 km. In order to determine if this width is real it is necessary to study the amount of errors in the hypocenters. As determined by HYPOINVERSE, the hypocentral location errors are approximately 120 meters horizontally and 175 meters vertically. In contrast the average errors for the Poley et al. (1987) data set are 270 meters horizontally and 400 meters vertically. This provides an additional objective measure of how retiming the earthquakes improves our ability to locate them. These are 67% confidence limits on the hypocenters in one dimension (e.g. distance from a plane) and refer to the coordinate system used by the location program and not to actual latitude, longitude, and depth. There are likely to be systematic differences between the two coordinate systems but these are not of interest when determining the width of the fault zone. Instead, we are only interested in the relative errors between hypocenters which are part of the errors given by HYPOINVERSE.

Figure 8 shows the distribution of distances between the hypocenters and the reference plane. Also shown is the best fitting gaussian distribution and the gaussian distribution that would correspond to the errors as determined by HYPOINVERSE. A χ^2 test reveals that there is over 99.5% confidence that the distribution of misfits does not come from a gaussian distribution. This implies that the 210 meters of rms misfit does not correspond to a process that produces gaussian errors. Interestingly the central maximum in the distribution is approximately 200 meters wide. This could correspond to a standard deviation in the locations of approximately 100 meters, which is the size of the errors determined by HYPOINVERSE. However, the distribution does not fall off rapidly enough away from the fault to be described by a gaussian. The relatively large number of events away from the fault demonstrate that the fault has a finite width. The shift between the central distribution and the gaussian distribution corresponding to the HYPOINVERSE errors suggests that this structure consists of off-fault

events to the southwest of a planar fault. An alternative explanation is that the earthquakes all lie on a plane and that the hypocentral location errors are not gaussian as modeled by HYPOINVERSE.

To further investigate this structure, the cross section in Figure 7 was divided into 6 sections by distance along the fault in Figure 9. In the southern section (boxes 1 to 3) the fault has no demonstrable width. This may be due to the fault being a simple plane, or that there are not enough events in this area to show the width. However, in the northern part of the region (particularly boxes 4 and 5), the fault zone is up to 1 km wide. This apparent width is unlikely to come from unmodeled velocity variations because much of the width comes from clusters of activity in a small part of the region (Figure 9). Therefore, for the width to be a product of unmodeled velocity variations, we would have to invoke very short wavelength features with large velocity variations. It is also important to note that there is an area with a cluster of events and no apparent width to the fault. The September 1987 swarm is shown in box 1 of Figure 9 where a number of events all co-locate and show no width. This suggests that the location process is accurate enough to determine if the fault has width on the order of 1 km. This tight clustering is also supported by Foxall and McEvilly (1987) despite the fact that they used a completely different network of seismometers. To further test the locations within these clusters the events in boxes 1, 4, and 5 were relocated with a subset of the stations such that the events in each box were recorded on the same set of stations. The patterns revealed in Figure 9 were largely unchanged.

The 6 boxes were chosen to divide up the fault without dividing up any of the obvious clusters of seismicity. This left boxes 4 and 5 with the greatest size and number of events. To demonstrate that this is not the reason the fault is widest in these boxes we now investigate the relationship between the location errors and locations in boxes 1, 4, and 5. In Figure 10 the distributions of misfit to the reference plane are shown for the events in the three clusters. In the box 1 cluster the gaussian distributions for both the rms misfits and the HYPOINVERSE errors seem to adequately explain the data. This implies that in an area where the fault is planar the misfit of the data to the reference plane can be described by the errors given by HYPOINVERSE. However, in boxes 4 and 5 the data are decidely not described by a gaussian distribution and even more obviously not by the gaussian

distribution corresponding to the HYPOINVERSE errors. Taken in contrast to the results from box 1 this suggests that the clusters in boxes 4 and 5 do show that the fault has demonstrable width.

Thus, three conclusions can be reached. The first is that the fault zone is not a simple plane and the second is that it may widen toward the north. The third is that this pattern is on the edge of resolution with these techniques and would not be resolvable from the catalog phase data before retiming.

FAULT PLANE SOLUTIONS

For the final chosen velocity model and station corrections fault plane solutions were calculated using FPFIT (Reasenberg and Oppenheimer, 1985). FPFIT uses a 2-stage, 3-D grid search procedure to minimize the normalized weighted sum of first motion polarity discrepancies. Alternate solutions are also calculated; these solutions and station discrepancies have been checked, and the best solution was used for each event. On the average, 21 stations were used for each fault plane solution. FPFIT also computes 90% confidence regions based on a priori estimates of the errors in the data.

The 71 fault plane solutions are shown in Figure 11. The expected solution for the San Andreas fault is right lateral motion on a vertical fault plane parallel to the surface strike of the fault. 69 of the determined fault plane solutions are consistent with this focal mechanism within 90% confidence. This is in direct contrast to the results from Seeber and Armbruster's (1988) analysis of the standard catalog phase data. They stated that almost half of the fault plane solutions could not be the expected solution for the San Andreas fault. While their study covered a much longer area along the San Andreas fault near Parkfield they did not single out this region as one of unusual simplicity. As stated in the methods section the greatest difference between our retimed data and the standard catalog phase data is the addition of P-wave picks on stations not read during the compilation of the standard catalog. This provides greater constraints on the fault plane solutions and we suspect that this explains the differences between their results and those presented here.

The other two mechanisms are a pure thrust (event 43) and an oblique thrust with a component of right lateral motion on the San Andreas (event 13). The latter event appears to allow a San Andreas

style solution, however this is not allowed within the 90% confidence limits and no alternate solution was found by FPFIT. This constraint is largely based on one station, and hence the mechanism is subject to some doubt. The other thrust (event 43) has an alternate solution that is a north-northeast strike-slip (Figure 12). The alternate solution requires that we ignore station PCRM, however this station is on the upper hemisphere and therefore the takeoff angle and azimuth are very sensitive to the location and velocity structure and there are no other stations near PCRM to verify this first motion. This event is the hypocenter that is 2.5 km off the San Andreas and is the deepest event (13.42 km deep) of the 71 studied. Figure 13 shows 27 representative focal mechanisms and their associated epicenters. The dominance of strike-slip solutions is obvious. Events 9, 33 and 35 appear to show some normal faulting component, but can be pure strike-slips within 90% confidence. Only the thrust solutions toward the north end of the region can not be pure strike-slip on the San Andreas within 90% confidence.

DISCUSSION

The hypocenters and fault plane solutions determined in this paper generally outline a nearly vertical strike-slip fault. However, within that fault there are complications both in structure and focal mechanism. The seismicity clusters on the plane (Figure 7) as suggested by Poley et al. (1987) and we suggest that the fault has a finite width of up to 1 km that may vary along strike.

Another complication is the 5° bend in the fault at the location of the 1966 main shock proposed by Lindh and Boore (1981). In a reanalysis of the 1966 Parkfield aftershock data, Lindh and Boore (1981) looked at the polarities of P-wave first motions on the stations at Gold Hill and Parkfield. Polarities at both the Gold Hill station (GDH, now PGHM) and the Parkfield station (PKF, now PPFM) of every well-located aftershock from Eaton et al. (1970) showed dilatations for epicenters north of the main shock region and compressions for epicenters to the south. Polarities of these stations showed dilatations for epicenters south of Gold Hill. Their explanation for these polarity changes is a 5° change in orientation of the fault plane near the main shock epicenter.

In order to see if this pattern continued after the 1966 aftershock sequence, we examined our data set of 71 earthquakes as well as the catalog data starting from 1969 and continuing to the present. In

this case it is acceptable to use the catalog data. As stated earlier, retiming the data rarely found errors in the P-wave polarities that had been picked. Figure 14 shows our results. Tables 2A and 2B show these results as compared to Lindh and Boore (1981). We did find that this pattern continues, though it is a noisy pattern. We do not believe that errors in reading first motions in the catalog alone can account for the noise in this pattern, instead it may be related to error in the hypocenters of the earthquakes, or complexity in fault itself.

In the final location map (Figure 5), a bend in the seismicity similar to their proposed bend can be seen. However, this is an artifact of projecting the hypocenters which occur on a dipping fault to the surface. In the cross-section taken along the fault (Figure 6), it is clear that most of the deep earthquakes occur near Middle Mountain in the center of the region studied. When combined with the 86° dip of the fault shown in Figure 7, this pattern will appear as a non-linear fault trace in map view.

To further test if the 5° bend could be seen in the hypocentral locations the seismicity was broken into two groups north and south of the proposed bend. Then the best fitting plane was found for each group by minimizing the least-square horizontal misfit to the reference plane. The group to the north showed a strike of 43° W of N with a dip of 87° to the NE. The southern group showed an almost identical orientation with a strike of 44° W of N with a dip of 85° to the NE. The use of non-parametric bootstrap statistics demonstrates change in strike is -1° with a 95 confidence range from -5° to 2°. Thus the proposed 5° bend is not evident in the hypocentral locations. We also applied this analysis to the Poley et al. (1987) data set and found a very different result. Their data set suggests a -8° rotation with a 95% confidence range from -13° to 2°. The best fitting rotation (-8°) from their locations is not within the 95% confidence range from our data and is largely due to mislocation of earthquakes in the area north of Middle Mountain. The larger confidence range determined from their hypocenters also shows the effects of using the catalog data. It is not that their hypocenters are wrong, only that using the catalog data limits the scale at which analysis can succeed.

This lack of a demonstrable rotation in the hypocenters leaves a paradox. The P-wave first motions at Parkfield and Gold Hill show a noisy but unambiguous pattern that can be explained by a 5° bend in the fault at Middle Mountain. However, this bend is not apparent in the hypocenters. Several

possible solutions to this paradox exist. Although a simple refraction across the fault, caused by different velocity structure on the two sides of the fault, cannot explain the first motion data (Lindh and Boore, 1981), more complicated velocity models with variations in all three dimensions might be able to. Another possibility is that the San Andreas is an imbricated fault. Then the orientation of the individual facets, which control the first motion data, could change without affecting the overall direction of the fault, which controls the hypocentral locations. An imbricated fault could also explain the large amount of scatter in the first motion data. Both of these explanations are more complicated than the simple bend proposed by Lindh and Boore (1981), but the data seem to require this.

As discussed in the previous section, 69 of the 71 fault plane solutions we determined showed the expected strike-slip focal mechanisms. The one indisputable fault-normal compression event occurred 2.5km NE of the San Andreas fault at a depth of 13.42 km, the deepest in our data set. The event could be related to the thrust structures east of the San Andreas fault, though most of these thrusts are believed to be shallow features (John Sims, personal communication, 1988). Another possibility is that this event represents an extension of one of the north-south trending basement structures that have been seen in gravity data and surficial geology at Coalinga (Carl Wentworth, written communication, 1988). These structures run through the "quiet zone" seen in aftershocks of the 1983 Coalinga earthquake where north-south strike-slip mechanisms similar to the alternate solution have been observed (Eaton, 1985). In either case, this event indicates some amount of fault-normal compression (e.g. Zoback et al., 1987, Oppenheimer et al., 1988). The other thrust event, which could possibly be a San Andreas style event, co-locates with the strike-slip solutions in the northern part of the region and is a shallow event.

However, while the fault-normal compression event is an interesting and important anomaly we should emphasize that almost all of the events are strike-slip solutions. The two thrust or oblique thrust mechanisms both occur toward the northern end of the region. This is close to the transition between the Parkfield rupture zone and the creeping section of the San Andreas to the northwest. The change in mechanism could represent an anomaly in the stress field with more fault normal compression in this area. As such it could be causally related to the northwest termination of the 1966 rupture and the change in faulting style from the Parkfield characteristic earthquakes to the aseismic creep observed

north of this point. This would be similar to the stress anomaly found by Jones (1987) at the southern termination of the 1857 Fort Tejon earthquake's rupture zone. However, given the small number of anomalous fault plane solutions this is only speculation. It is also possible that the basement tear running from Coalinga to Middle Mountain is responsible for the change in fault behavior at Middle Mountain. A similar idea was proposed by Bakun and Lindh (1985). On the northeast side of the fault, they noted a difference between the surface rocks adjoining the fault in the creeping versus the locked sections. The problem with their suggestion is that the geologic differences they cite are shallower than the seismicity, while the suggested tear running from Coalinga to Middle Mountain may extend to seismogenic depths.

In order to identify more fault-normal compression events, the entire Parkfield seismicity catalog from 1969 to the present was relocated and new focal mechanisms were determined for 862 events. This process identified only 11 anomalous events. However, even after retiming the events from analog records, none of these were indisputably thrust or north-south strike-slip events. This is due to the lower station density in the earlier years. One intriguing observation was that most of the possible thrusts were in the northern end of the Parkfield rupture zone near Middle Mountain. This would tend to support the conclusion that there are more thrust and oblique events in that part of the region. However, due to the lower station density in the earlier years, this can not be conclusively demonstrated. If anything this exercise makes us even more suspicious of fault plane solutions that use only the catalog phase data from earlier years (e.g. Seeber and Armbruster, 1988).

CONCLUSIONS

Retiming the events and developing new station corrections allowed us to reduce the rms traveltime residuals from 0.083 to 0.025 seconds, halfed the standard errors in the hypocenters, and produced seismicity that better clusetered along the San Andreas fault when compared to the results of Poley et al.(1987). However, the new data does not support any change in the velocity model developed by Nowack, Ellsworth, and Lindh (unpublished data, 1982). In general we found that retiming the events made a significant difference in our ability to accurately relocate the events and determine fault plane solutions. While the standard U.S.G.S. Northern California Seismic catalog phase

data represent an impressive body of work, retiming earthquakes allowed us to make finer scale interpretations. In particular none of the following conclusions could have resulted from an analysis of the catalog data.

Relocating the events using the new station corrections, the seismicity in the Middle Mountain region was found to be confined to within 1 1/2 kilometers of the San Andreas fault zone. The general deepening of seismicity toward the center of the Middle Mountain zone delineated by Poley et al. (1987) was also apparent in this study. Cross sections taken at an azimuth of 48° east of north (the best orientation to show the seismicity as a plane) revealed that the fault is dipping steeply at 86° to the northeast. In the northwest end of the study area the fault is approximately 1 km wider than would be expected from the hypocentral location errors, suggesting that the fault is not a single plane. The 5° bend as proposed by Lindh and Boore (1981) was detected in this study after analyzing the first-motion data of events from 1969 to the present using the catalog phase data. However, application of non-parametric bootstrap statistics to the new hypocenters exclude the existence of the bend at greater than the 95% confidence level. This suggests that a more complicated model is necessary to explain the first motion data.

Sixtynine of the fault plane solutions determined for the 71 earthquakes were strike-slip, as expected for the San Andreas fault. One of the events, located in the north end of the study area co-locates with the strike-slip solutions and is probably a thrust solution. One other earthquake, located 2 1/2 kilometers off the fault has a either thrust or N-S striking right lateral solution, and may be related to thrust structures in the area, or possibly north-south trending faults seen in basement structures northeast of this area at Coalinga. If it is a thrust, which is the more probable solution, then this event suggests that the thrust faults mapped in this region are not confined to the upper few kilometers, but instead extend from the surface to the maximum depth of seismicity. However, these faults have few earthquakes on them. In either case it represents some amount of fault-normal compression in the northern part of the study zone. This leads us to speculate that this could be related to a stress anomaly, which in turn may be causally related to the transition between the creeping and locked Parkfield sections of the San Andreas fault zone.

Acknowledgements We thank Al Lindh, Bill Ellsworth, Bill Bakun and Carl Wentworth for many helpful suggestions, John Sims for letting us use his geologic maps prior to publication, Fred Klein for his help with HYPOINVERSE, Dave Oppenheimer for his help with FPFIT, and Katie Poley and Al Lindh for allowing us to use their catalog locations prior to their publication, and Bill Bakun, Fred Klein and Paul Reasenberg for thoughtful reviews.

REFERENCES

Bakun, W.H., and A.G. Lindh, he Parkfield, California, earthquake prediction experiment, *Science, 229* , 619-624, 1985.

Bakun, W.H., and T.V. McEvilly, Recurrence models and Parkfield, California, earthquakes, *J. Geophys. Res., 89*, 3051-3058, 1984.

Bakun, W.H., K.S. Breckenridge, J. Bredehoeft, R.O. Burford, W.L. Ellsworth, M.J.S. Johnston, L. Jones, A.G. Lindh, C. Mortensen, R.J. Mueller, C.M. Poley, E. Roeloffs, S. Schultz, P. Segall, and W. Thatcher, Parkfield, California, Earthquake prediction scenarios and response plans, *U.S. Geol. Surv., Open-File Report, 87-192*, 45 pp, 1987.

Dibblee, T.W., Geologic map of the Coalinga quadrangle, Geologic maps of seventeen 15-minute quadrangles (1:62,500) along the San Andreas fault in the vicinity of King City, Coalinga, Panoche Valley, and Paso Robles, California, with index map, scale 1:62,500, *U.S. Geol. Surv, Open-File Report, 71-0087*, 17 sheets, 1971a.

Dibblee, T.W., Geologic map of the Parkfield quadrangle, Geologic maps of seventeen 15-minute quadrangles (1:62,500) along the San Andreas fault in the vicinity of King City, Coalinga, Panoche Valley, and Paso Robles, California, with index map, scale 1:62,500, *U.S. Geol. Surv, Open-File Report, 71-0087*, 17 sheets, 1971b.

Dibblee, T.W., Geologic map of the Priest Valley quadrangle, Geologic maps of seventeen 15-minute quadrangles (1:62,500) along the San Andreas fault in the vicinity of King City, Coalinga, Panoche Valley, and Paso Robles, California, with index map, scale 1:62,500, *U.S. Geol. Surv, Open-File Report, 71-0087*, 17 sheets, 1971c.

Dibblee, T.W., Geologic map of the San Miguel quadrangle, Geologic maps of seventeen 15-minute quadrangles (1:62,500) along the San Andreas fault in the vicinity of King City, Coalinga, Panoche Valley, and Paso Robles, California, with index map, scale 1:62,500, *U.S. Geol. Surv, Open-File Report, 71-0087*, 17 sheets, 1971d.

Dickinson, W.R., Structural relationships of the San Andreas fault system, Cholame Valley and Castle Mountain Range, California, *Geol. Soc. Am. Bull., 77*, 707-726, 1966.

Eaton, J.P., The May 2, 1983 Coalinga earthquake and its aftershocks: a detailed study of the hypocenter distribution and of the focal mechanisms of the larger aftershocks, Proceedings of Workshop XXVII, Mechanics of the May 2, 1983 Coalinga earthquake, *U.S. Geol. Surv. Open-File Report, 85-44*, 132-201, 1985.

Eaton, J.P., M.E. O'Neill, and J.N. Murdock, Aftershocks of the 1966 Parkfield-Cholame, California earthquake: a detailed study, *Bull. Seismol. Soc. Am., 60* , 1151-1197, 1970.

Efron, B, and R. Tibshirani, Bootstrap methods for standard errors, confidence intervals, and other measures of statistical accuracy, *Stat. Sci., 1*, 54-77, 1986.

Foxall, W, and T.V. McEvilly, The Parkfield downhole seismic array: preliminary analyses of microearthquakes, *Eos Trans. AGU*, abstract, 1987.

Jones, L.M., Focal mechanisms and the state of stress on the San Andreas fault in southern California,, *J. Geophys. Res., 93*, 8869-8891, 1988.

King, G.K., and J. Nabalek, Role of fault bends in the initiation and termination of earthquake rupture, *Science*, 984-987, 1985.

Klein, F.W., User's Guide to HYPOINVERSE, a program for VAX Computers to solve for earthquake locations, *U.S. Geol. Surv., Open-File Report, 85-515*, 53 pp,

Lindh, A.G., and D.M. Boore, Control of rupture by fault geometry during the 1966 Parkfield earthquake, *Bull. Seismol. Soc. Am., 71*, 95-116, 1981.

McEvilly, T.V., W.H. Bakun, and K.B. Casaday, The Parkfield, California earthquakes of 1966, *Bull. Seismol. Soc. Am., 57*, 1221-1244, 1967.

Oppenheimer, D.H., P.A. Reasenberg, and R.W. Simpson, Fault-plane solutions for the 1984 Morgan Hill, California, earthquake sequence: evidence for the state of stress on the Calaveras fault, *J. Geophys. Res., 93*, 9007-9026, 1988.

Poley, C.M., A.G. Lindh, W.H. Bakun, and S.S. Schulz, Temporal changes in microseismicity and creep near Parkfield, California, *Nature, 327*, 134-137, 1987 .

Reasenberg, P.A., and D. Oppenheimer, FPFIT, FPPLOT and FPPAGE: Fortran computer programs for calculating and displaying earthquake fault-plane solutions,

U.S. Geol. Surv., Open-File Report, 85-739, 109 pp, 1985.

Roecker, S.W., and W.L. Ellsworth, VELEST Fortran Program, *U.S. Geological Survey*, Menlo Park, California., 1978.

Seeber, L., and J.G. Armbruster, Stress Orientation Inferred from the kinematics of secondary faults within the San Andreas fault zone at Parkfield, *Eos Trans. AGU, 69*, abstract, 1988.

Sims, J.D., Geologic map of the San Andreas fault zone in the Parkfield quadrangle, Monterey county, California, *U.S.G.S. Misc. Field Investigation Map, MF-xxxx*, 1988a.

Sims, J.D., Geologic map of the San Andreas fault zone in the Cholame Valley and Cholame Hills quadrangles, San Luis Opispo and Monterey counties, California, *U.S.G.S. Misc. Field Investigation Map, MF-1995*, 1988b.

Zoback, M.D., M.L. Zoback, V.S. Mount, J. Suppe, J.P. Eaton, J.H. Healy, D. Oppenheimer, P. Reasenberg, L. Jones, C.B. Raleigh, I.G. Wong, O Scotti, and C. Wentworth, New evidence on the state of stress of the San Andreas fault system, *Science, 238*, 1105-1111, 1987.

FIGURE CAPTIONS

Figure 1. Generalized map of the Parkfield area showing the location of the San Andreas fault zone and Middle Mountain. The Middle Mountain alert zone is represented by the polygon. Triangles represent seismic stations used in locations of earthquakes; more distant stations were used only for the fault plane solutions and are not shown.

Figure 2. Examples of seismic trace outputs from the CUSP system. Weights of 0 to 3 for P wave arrival picks are shown.

Figure 3. Earthquakes used in this study showing (A) locations of Poley et al. (1987) and (B) locations after retiming. Note that to show the structure of the seismicity more clearly the earthquake symbols are not scaled to the magnitude of the earthquake. The polygon represents the Middle Mountain alert zone. The San Andreas fault (simplified) is represented by the diagonal line.

Figure 4. Velocity model developed by Nowack et al. (unpublished data, 1982) (thick line) and the velocity model developed in this study using VELEST (thin line). The models are the same below a depth of 15 kilometers.

Figure 5. (A) Locations of earthquakes after retiming and relocating using new station corrections. (B) shows the same locations on a map where detailed fault structure has been added. Cross-sections A-A' and B-B' are also shown.

Figure 6. Cross-section, with no vertical exaggeration, taken along A-A' looking northeast (see Figure 5B) showing locations of earthquakes using the new station corrections. Middle Mountain is located about 12 kilometers from point A. The 1966 foreshock (small star) and main shock (large star) are also shown.

Figure 7. Cross-section, with no vertical exaggeration, taken along B-B' looking northwest (see Figure 5B) showing locations of earthquakes using the new station corrections. The line represents

the best fitting plane. The earthquake at 13.42 kilometers depth was not used in the plane fitting.

Figure 8. Distribution of horizontal distances between the hypocenters and the best fitting plane. The lighter gaussian curve corresponds the best fitting gaussian distribution to the data. The darker gaussian corresponds to the distribution expected from the horizontal location errors as determined by HYPOINVERSE.

Figure 9. Map and cross sections showing locations of earthquakes using new station corrections. Boxes show location of cross sections taken perpendicular to the fault looking northwest (parallel to B-B' in Figure 5B) at an angle of 48 degrees east of north. The 1966 main shock is represented by the star in box 3.

Figure 10. Distribution of horizontal distances between the hypocenters and the best fitting plane for the clusters of seismicity in boxes 1, 4, and 5. The lighter gaussian curve corresponds the best fitting gaussian distribution to the data. The darker gaussian corresponds to the distribution expected from the horizontal location errors as determined by HYPOINVERSE.

Figure 11. A and B quality fault plane solutions. Solid circles represent compressions, open circles represent dilatations. Numbers correspond to those in Table 1.

Figure 12. Fault plane solutions for the deep earthquake (number 43), with the best solution shown on the left of the alternate solution.

Figure 13. Map showing representative fault plane solutions Numbers correspond to the fault plane solutions in Figure 9, and earthquakes listed in Table 1.

Figure 14. Plot of events from 1969 to the present where different symbols show first motions at Parkfield (PPFM) and Gold Hill (PGHM). Events were shown only if both stations had up first motions or both had down first motions. Boxes A, B and C are referred to in Tables 2A and 2B.

Table 1. List of earthquakes studied.

NUM	DATE	ORIGIN	LAT	LONG	DEPTH	MAG	RMS	DIR	DIP	RAKE
1	840420	1115 32.28	35-59.77	120-32.73	4.74	1.50	0.02	40	90	175
2	840809	1557 50.49	35-58.85	120-31.32	11.49	1.90	0.03	230	60	180
3	840811	0148 33.47	35-58.95	120-31.72	11.83	1.50	0.02	235	50	-170
4	840811	0534 38.91	35-58.89	120-31.76	11.60	1.50	0.03	235	60	-179
5	840812	0655 15.58	35-58.89	120-31.45	11.51	1.80	0.03	230	55	180
6	840813	0552 58.85	35-58.58	120-31.05	7.75	1.50	0.02	235	70	-170
7	840924	1856 32.66	35-55.87	120-28.31	5.18	1.70	0.04	236	80	-169
8	841006	0029 16.89	35-59.65	120-32.48	5.23	1.80	0.01	37	60	-174
9	841124	1243 41.34	35-58.32	120-30.82	11.38	1.90	0.03	245	45	-160
10	841127	2338 13.05	35-55.72	120-28.28	4.74	1.70	0.04	50	75	180
11	850201	0256 21.44	36-00.64	120-33.74	5.67	2.00	0.02	43	61	157
12	850201	0457 34.07	35-58.70	120-31.47	7.17	1.80	0.02	230	50	-170
13	850214	1329 18.20	36-00.52	120-33.44	5.02	2.60	0.02	30	33	151
14	850312	1044 59.64	35-58.31	120-31.28	11.81	0.90	0.01	240	35	-150
15	850315	1237 01.40	35-58.53	120-31.08	11.61	1.60	0.02	225	50	-170
16	850327	1254 30.23	35-59.84	120-33.32	4.52	1.90	0.02	45	70	180
17	850407	1813 14.55	36-00.86	120-33.56	10.64	1.60	0.00	270	40	-170
18	850422	2318 34.32	36-00.85	120-33.96	5.37	1.90	0.03	50	75	160
19	850518	1506 45.11	35-57.42	120-29.97	11.85	1.70	0.05	45	90	180
20	850525	0030 22.93	35-56.46	120-28.71	10.57	1.20	0.03	234	67	135
21	850525	0419 38.70	35-56.47	120-28.71	10.28	2.80	0.03	240	90	175
22	850[illegible]0	1221 56.90	35-59.77	120-33.55	4.36	1.60	0.06	230	85	180
23	850608	0145 59.35	35-58.12	120-30.74	7.79	1.80	0.01	210	75	180
24	850712	0047 21.93	35-59.85	120-32.95	3.03	3.00	0.03	39	60	168
25	850808	0458 42.06	36-00.03	120-33.08	5.07	2.00	0.01	40	80	-174

26	851103	1817 51.92	35-57.45	120-30.46	7.73	1.00	0.01	240	35	-160
27	851111	2056 18.14	35-57.03	120-29.38	11.45	1.30	0.03	240	60	170
28	851214	1442 39.44	36-00.03	120-32.99	4.74	1.70	0.01	45	85	170
29	851215	0014 29.79	35-59.74	120-32.78	5.36	1.80	0.02	43	80	169
30	851216	0157 56.49	36-00.01	120-32.99	4.80	1.80	0.01	45	85	180
31	851222	2045 34.74	35-56.23	120-28.73	5.60	1.80	0.02	40	70	179
32	860128	0710 04.31	35-58.20	120-30.71	11.30	1.90	0.02	225	70	-179
33	860201	0346 51.48	35-58.10	120-30.80	11.43	1.40	0.01	245	24	-141
34	860224	0144 25.92	36-00.08	120-33.11	3.09	2.20	0.02	40	40	179
35	860402	0555 43.03	35-58.30	120-30.76	11.18	2.00	0.02	240	35	-160
36	860419	1910 36.86	35-58.88	120-32.27	4.23	1.90	0.03	24	70	164
37	860512	0956 37.55	36-00.23	120-33.30	4.88	2.10	0.02	31	50	167
38	860519	1758 12.02	36-00.74	120-34.07	5.19	2.40	0.03	40	90	165
39	860519	1801 09.19	36-00.69	120-33.98	5.37	1.70	0.03	40	90	165
40	860520	0819 44.12	36-00.17	120-33.17	4.93	2.00	0.01	44	80	174
41	860610	2010 31.39	35-59.12	120-32.14	2.88	2.20	0.03	34	60	168
42	860804	1722 03.33	35-57.55	120-30.07	9.08	1.70	0.01	240	50	-160
43	861010	0713 07.49	36-00.02	120-31.38	13.42	1.70	0.03	55	50	90
44	861119	0030 19.41	35-55.73	120-28.34	4.86	1.70	0.02	63	70	-169
45	870201	1125 33.01	35-57.77	120-30.30	5.32	1.60	0.02	38	80	169
46	870202	0445 00.99	35-55.77	120-28.01	10.06	2.50	0.04	55	90	175
47	870203	1449 33.39	35-55.76	120-27.90	10.14	1.40	0.03	240	80	-179
48	870314	1417 00.34	35-58.37	120-30.65	11.42	1.70	0.03	240	75	-160
49	870322	1902 28.82	35-59.99	120-33.16	3.35	1.70	0.03	50	90	180
50	870322	1944 22.77	36-00.05	120-33.05	3.12	1.80	0.02	39	60	168
51	870327	1303 00.52	35-58.28	120-31.00	11.37	1.50	0.03	238	50	-167
52	870413	0659 09.57	36-00.05	120-33.17	5.00	2.20	0.02	36	61	162

53	870428	1916 55.85	35-58.42	120-30.56	11.66	2.10	0.03	234	80	174
54	870503	1828 03.97	36-00.04	120-33.18	3.99	1.70	0.08	31	50	167
55	870504	0310 03.66	35-59.98	120-33.02	4.88	1.70	0.02	43	80	169
56	870507	0310 02.08	35-55.82	120-28.40	4.89	1.50	0.02	50	80	180
57	870509	1708 13.83	35-55.87	120-28.37	5.46	1.80	0.02	46	70	-174
58	870530	1358 09.24	35-59.94	120-33.32	3.79	1.70	0.04	43	80	169
59	870531	1603 41.22	35-59.50	120-32.45	5.08	1.60	0.02	39	81	149
60	870618	0142 58.21	35-57.56	120-30.62	2.84	1.50	0.05	11	70	169
61	870807	0425 56.02	35-56.83	120-28.70	10.54	2.10	0.05	238	80	169
62	870828	2039 11.59	35-58.66	120-31.13	11.00	2.10	0.01	220	50	-179
63	870918	1050 28.17	35-55.44	120-27.96	5.44	1.60	0.02	45	85	170
64	870918	1050 40.26	35-55.40	120-28.01	5.32	1.50	0.03	218	80	-159
65	870918	1055 05.09	35-55.47	120-28.01	5.43	1.90	0.02	45	80	179
66	870918	1056 17.43	35-55.45	120-28.05	5.46	1.30	0.02	45	90	170
67	870918	1057 34.66	35-55.47	120-27.97	5.47	1.50	0.02	50	85	170
68	870919	0002 31.33	35-55.45	120-28.02	5.47	1.80	0.02	40	80	179
69	870919	0235 25.52	35-55.42	120-28.02	5.58	1.40	0.02	225	85	180
70	870919	0347 57.28	35-55.54	120-28.11	5.08	1.40	0.01	43	80	169
71	870926	1743 50.67	35-55.75	120-28.39	4.77	1.40	0.02	50	85	-170

NUM is the number of earthquake as referred to in text. DATE is in the form yymmdd; where yy=year, mm= month, and dd=date. ORIGIN is the origin time in the form hhmm sec; where hh=hour, mm=minute, sec=seconds in GMT. LAT is the epicentral latitude in degrees-minutes north. LONG is the epicentral longitude in degrees-minutes west. DEPTH is the focal depth in kilometers. MAG is the local Richter magnitude. RMS is the rms residual travel time in seconds DIR is the dip direction of the fault plane. DIP is the dip of the fault plane. RAKE is the rake of the focal mechanism.

Table 2A. First Motion Data from PGH.

	Box A	Box B	Box C
Catalog Data 1969-present	65% Down (165)	71% Up (238)	66% Down (85)
Data Set- This Study	62% Down (13)	57% Up (14)	-
Lindh and Boore(1981)	91% Down	95% Up	88% Down

Numbers in parentheses refer to total number of data points used.

Table 2B. First Motion Data from Gold Hill and Parkfield.

	Box A	Box B	Box C
Catalog Data 1969-present	80% Down (88)	80% Up (89)	70% Down (47)
Data Set- This Study	87% Down (8)	100% Up (6)	-
Lindh and Boore(1981)	100% Down	100% Up	-

First motions on both stations up or down. Numbers in parentheses refer to total number of data points used.

PARKFIELD REGION

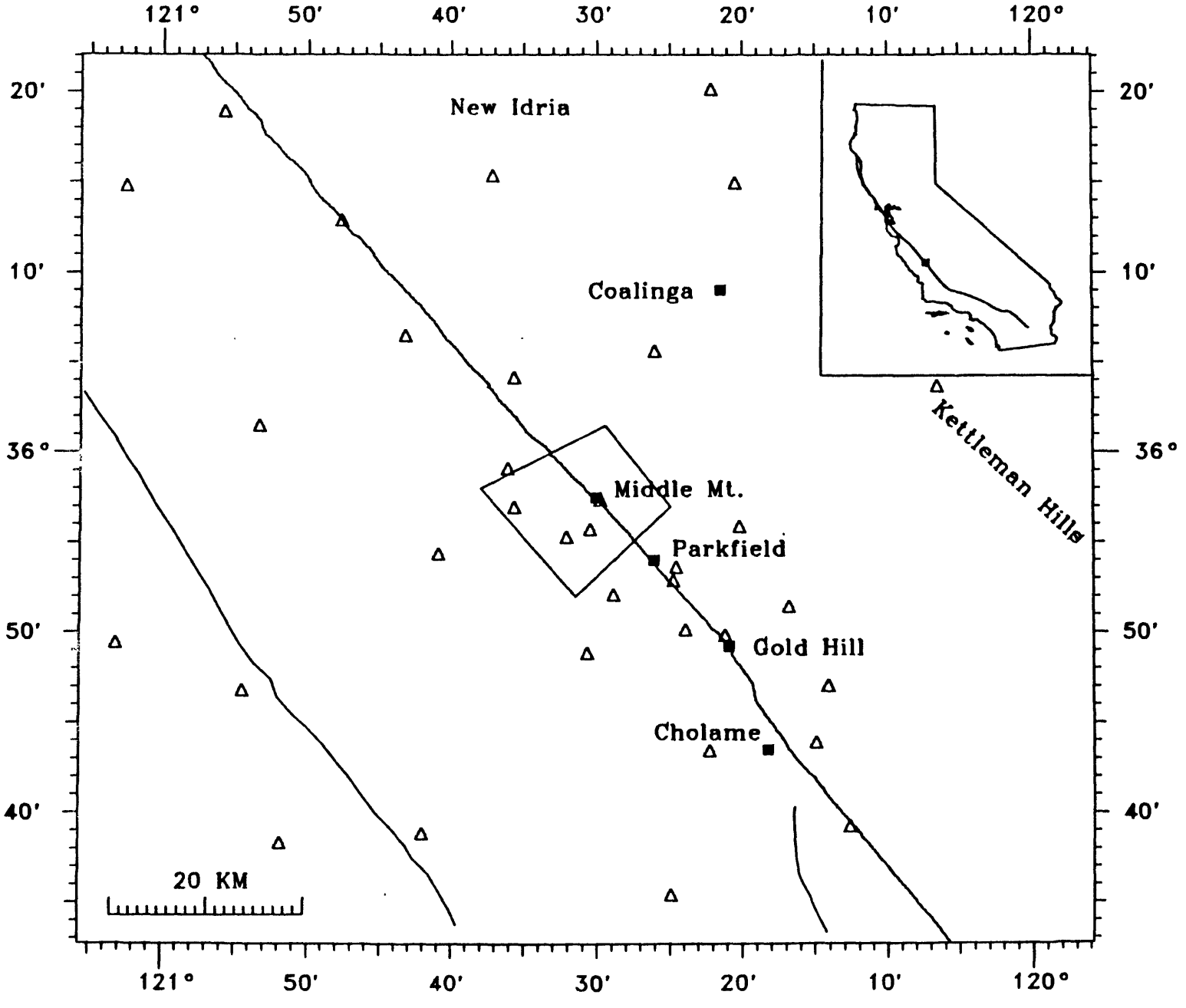

Figure 1

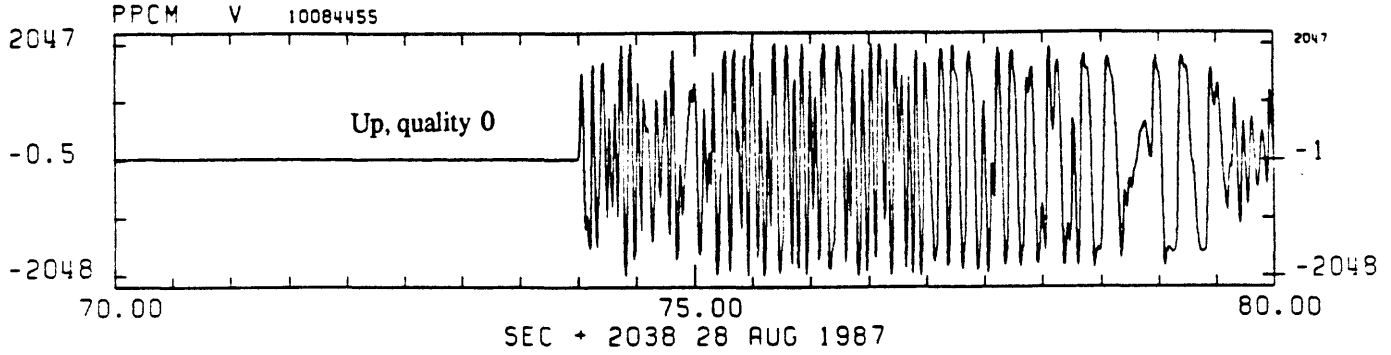
PPCM V 10084455
2047
-0.5
-2048
Up, quality 0
2047
-1
-2048
70.00
75.00
80.00
SEC + 2038 28 AUG 1987

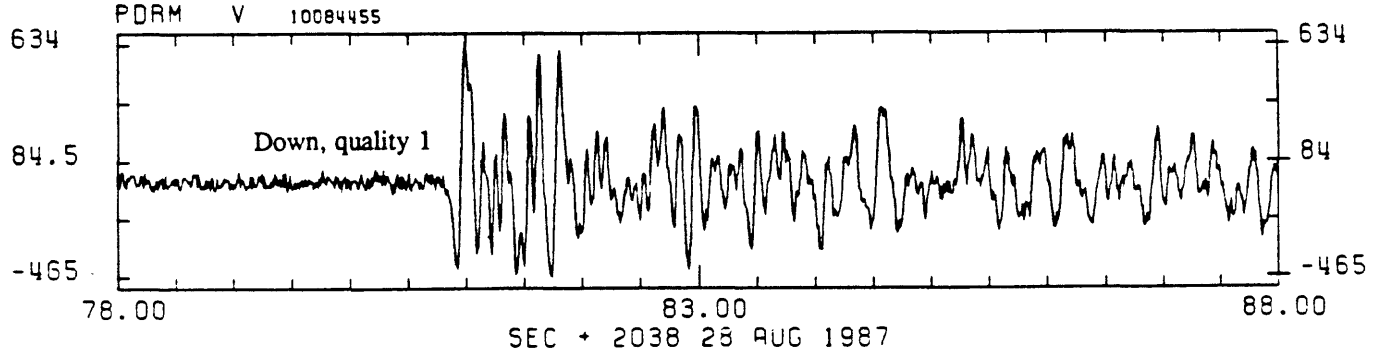
PDRM V 10084455
634
84.5
-465
Down, quality 1
634
84
-465
78.00
83.00
88.00
SEC + 2038 28 AUG 1987

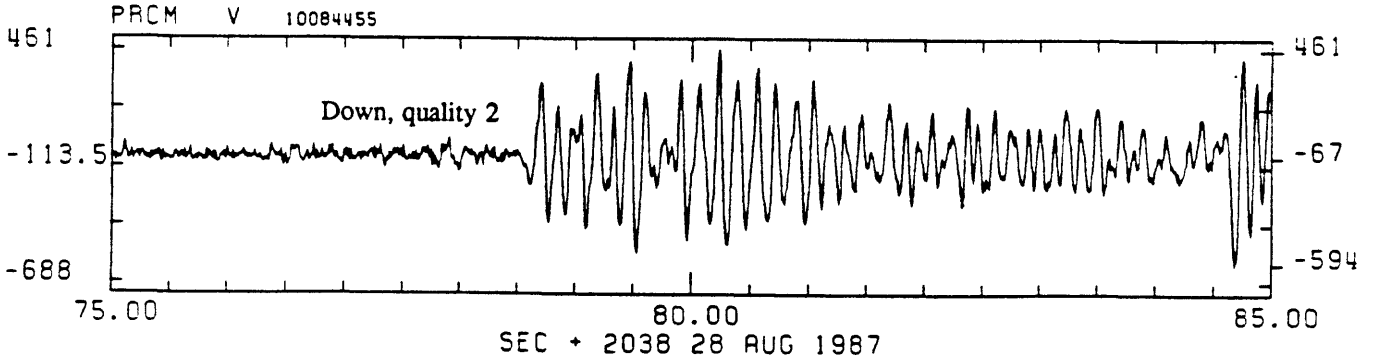
PRCM V 10084455
461
-113.5
-688
Down, quality 2
461
-67
-594
75.00
80.00
85.00
SEC + 2038 28 AUG 1987

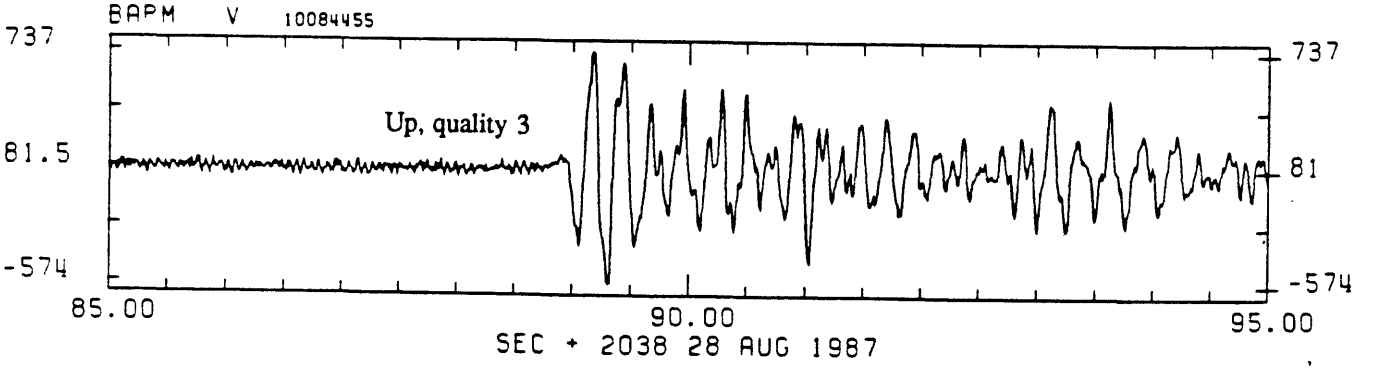
BAPM V 10084455
737
81.5
-574
Up, quality 3
737
81
-574
85.00
90.00
95.00
SEC + 2038 28 AUG 1987

Figure 2

MIDDLE MOUNTAIN SEISMICITY
CATALOG LOCATIONS

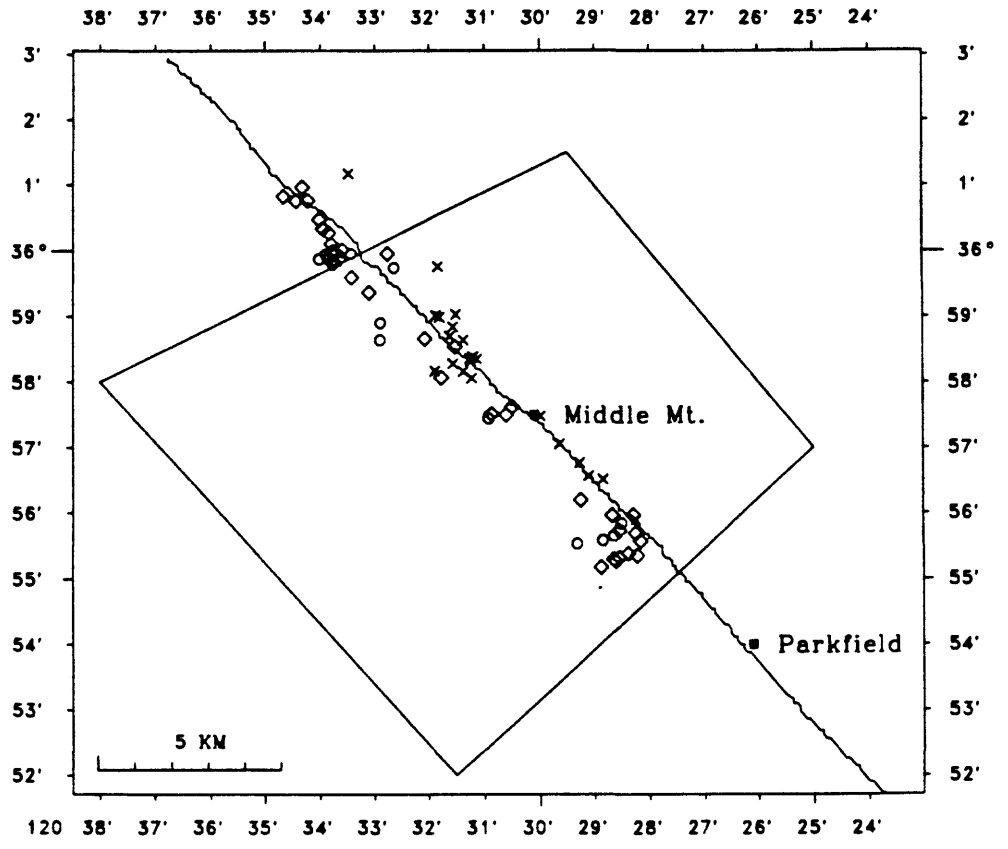

MIDDLE MOUNTAIN SEISMICITY
LOCATIONS AFTER RETIMING

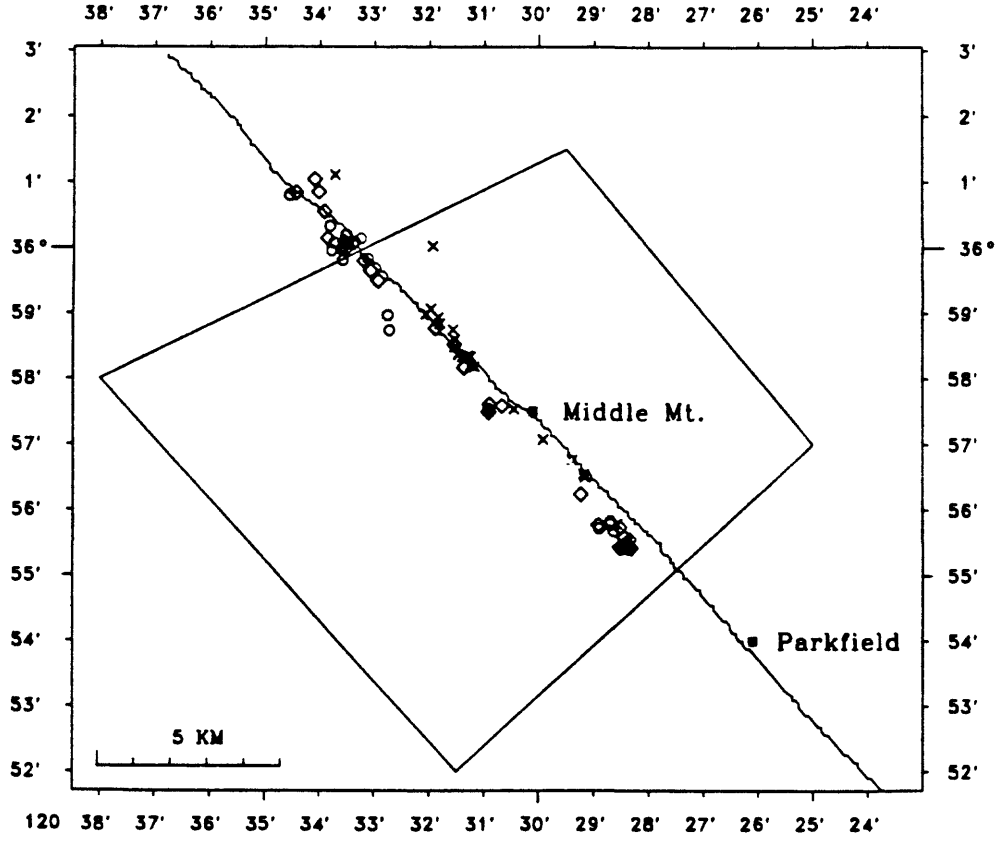

Figure 3

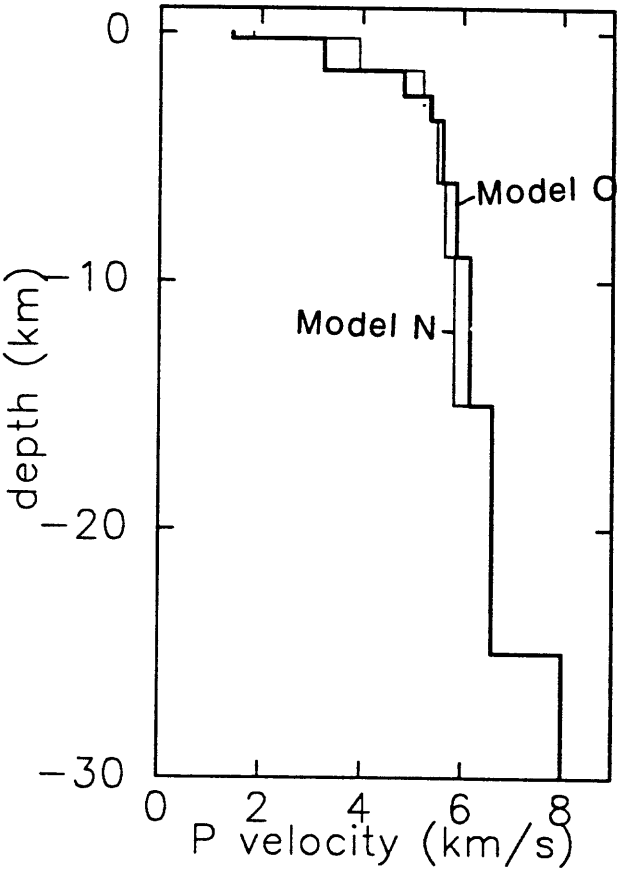

Figure 4

MIDDLE MOUNTAIN SEISMICITY
LOCATIONS WITH NEW STATION CORRECTIONS

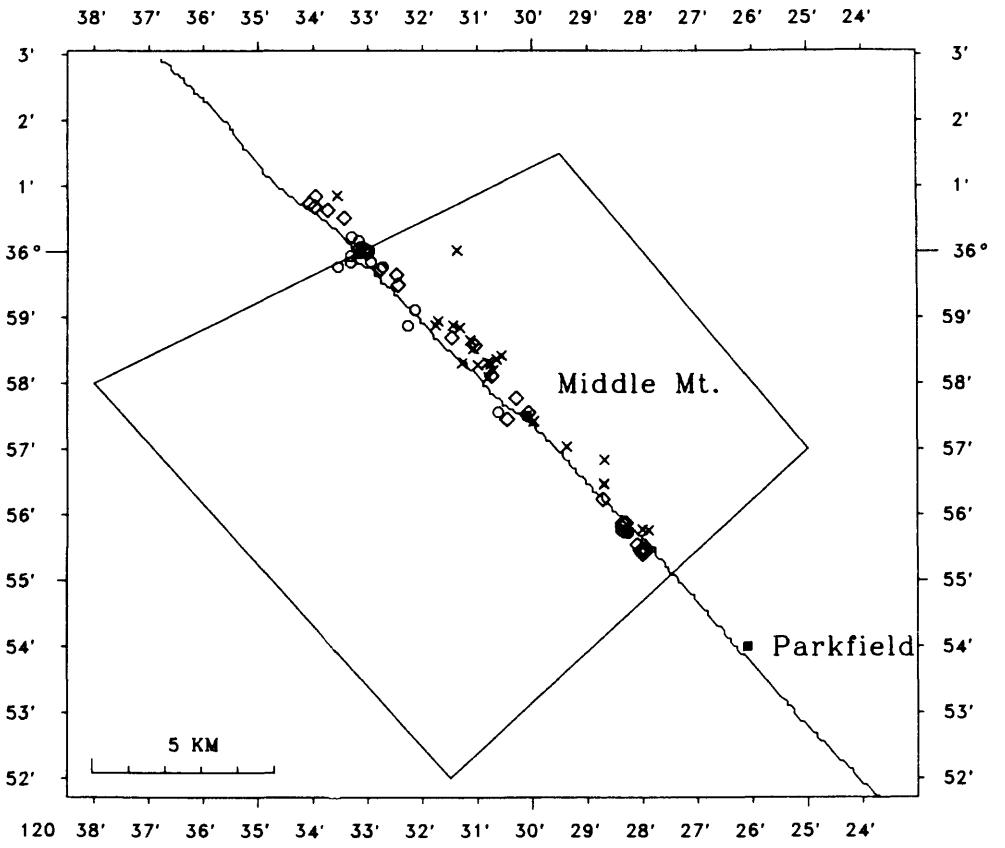

MIDDLE MOUNTAIN SEISMICITY
LOCATIONS WITH NEW STATION CORRECTIONS

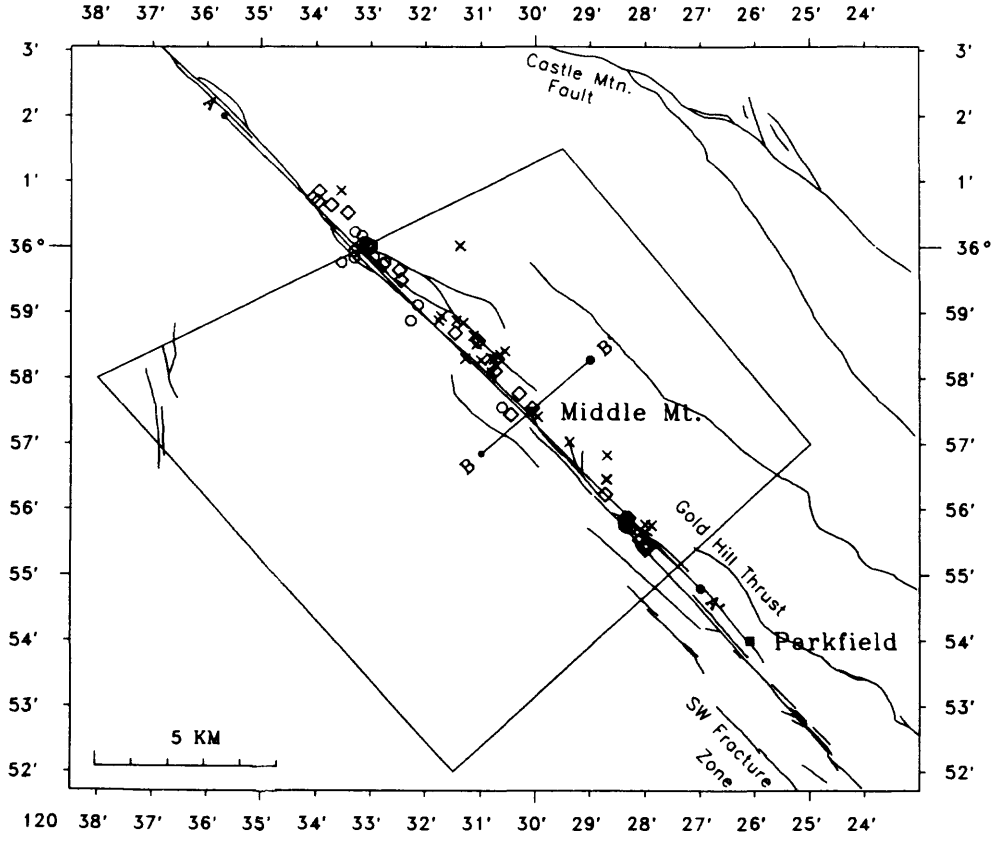

Figure 5

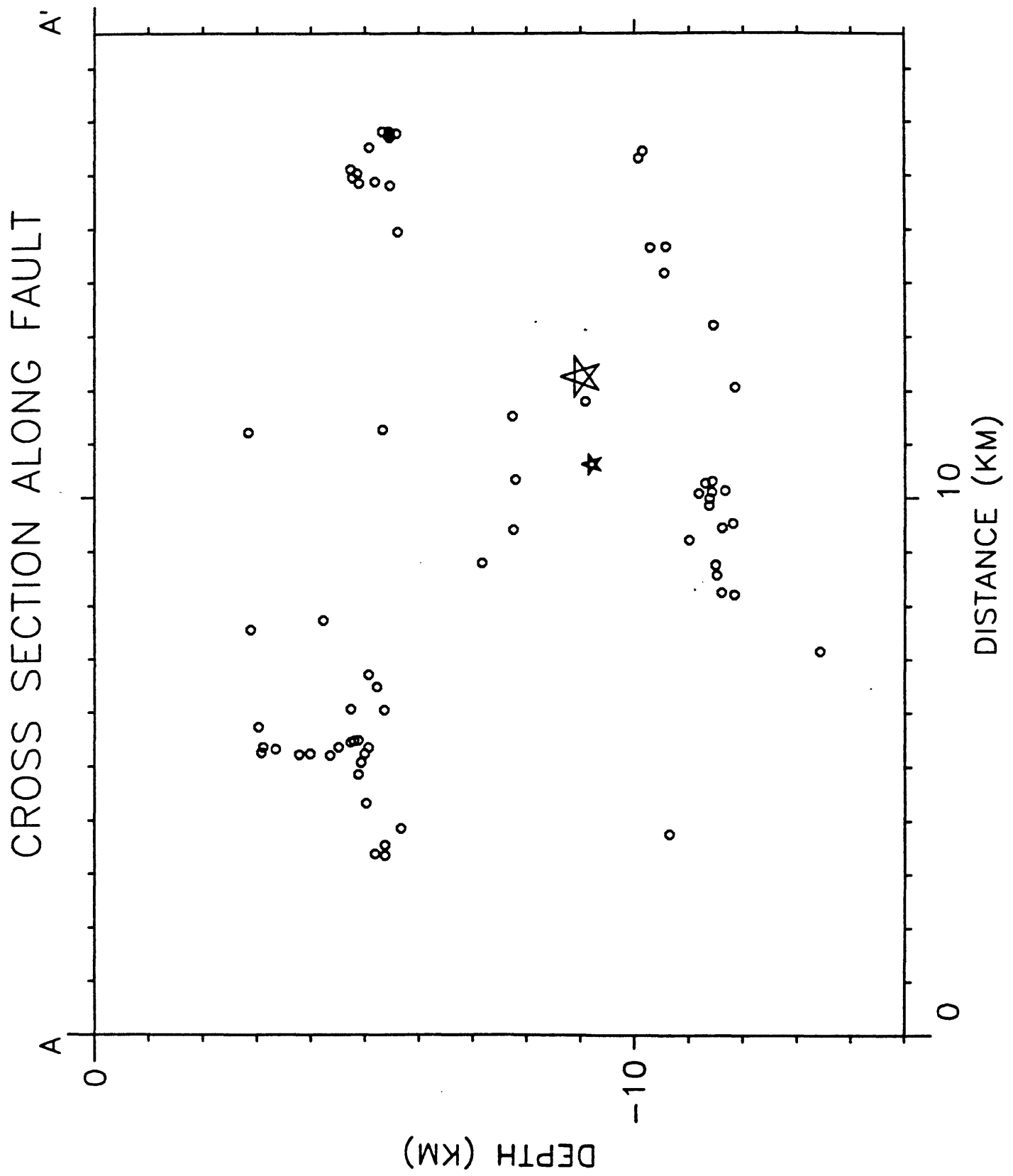

Figure 6

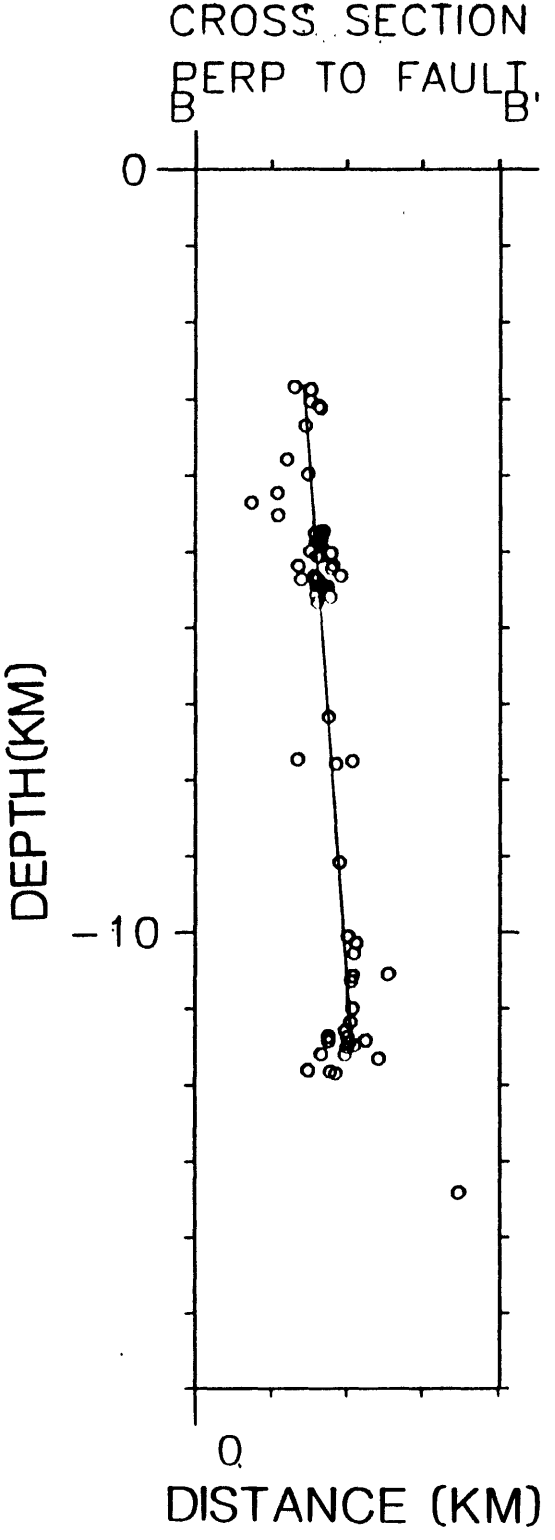

Figure 7

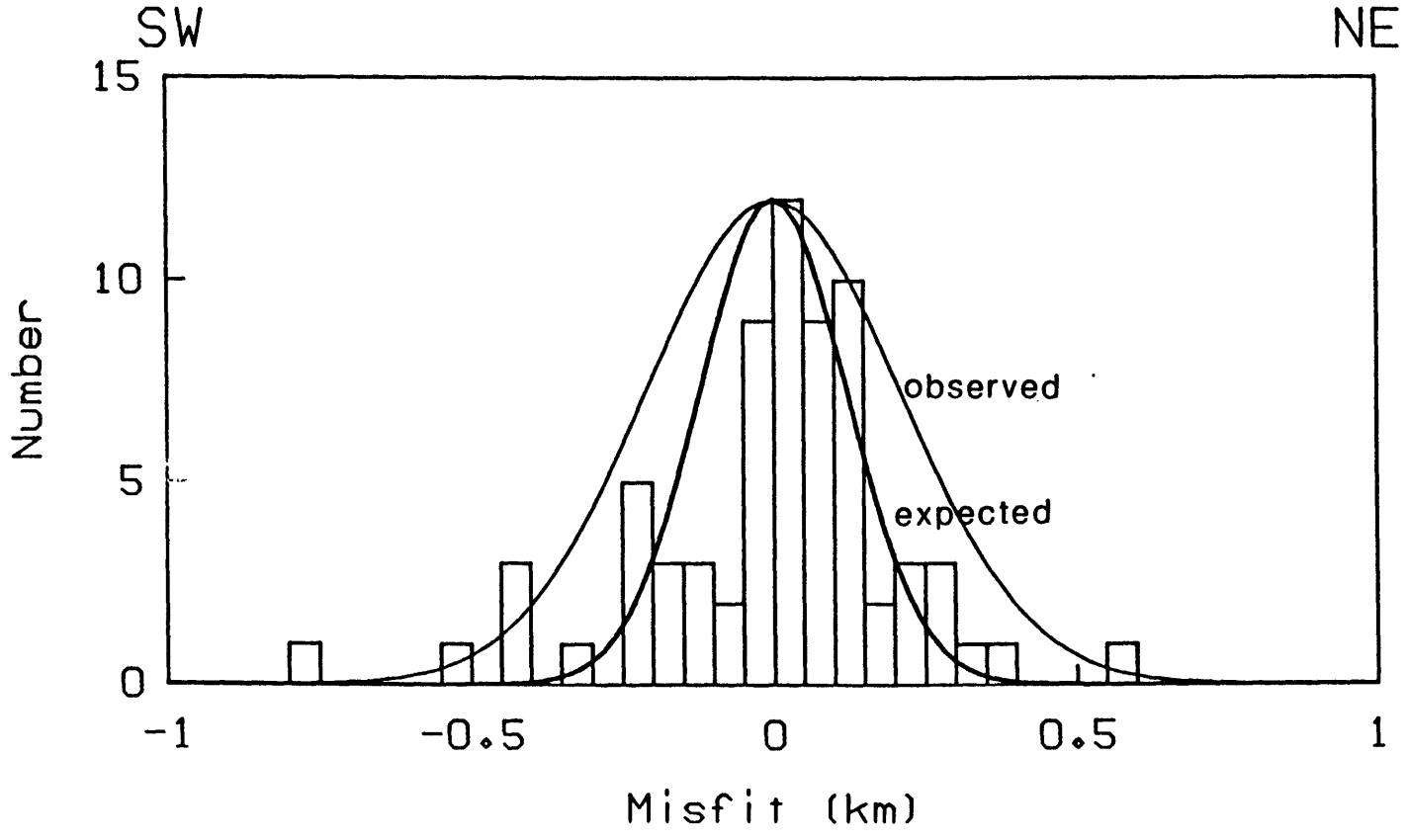

Figure 8

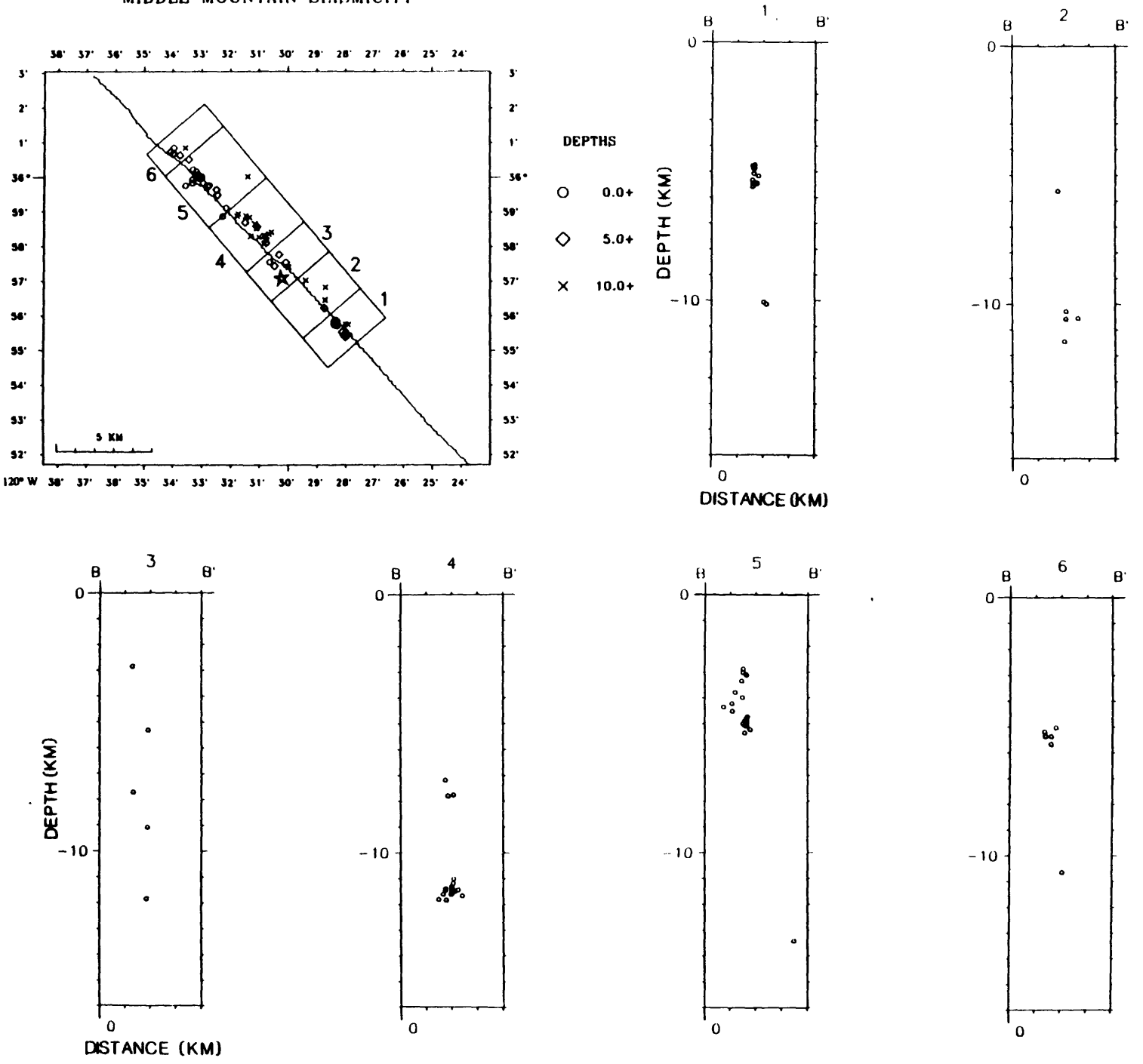
MIDDLE MOUNTAIN SEISMICITY
5 KM
DEPTHS
0.0+
5.0+
10.0+
DEPTH (KM)
DISTANCE (KM)
B
B'
1
2
3
4
5
6
0
-10

Figure 9

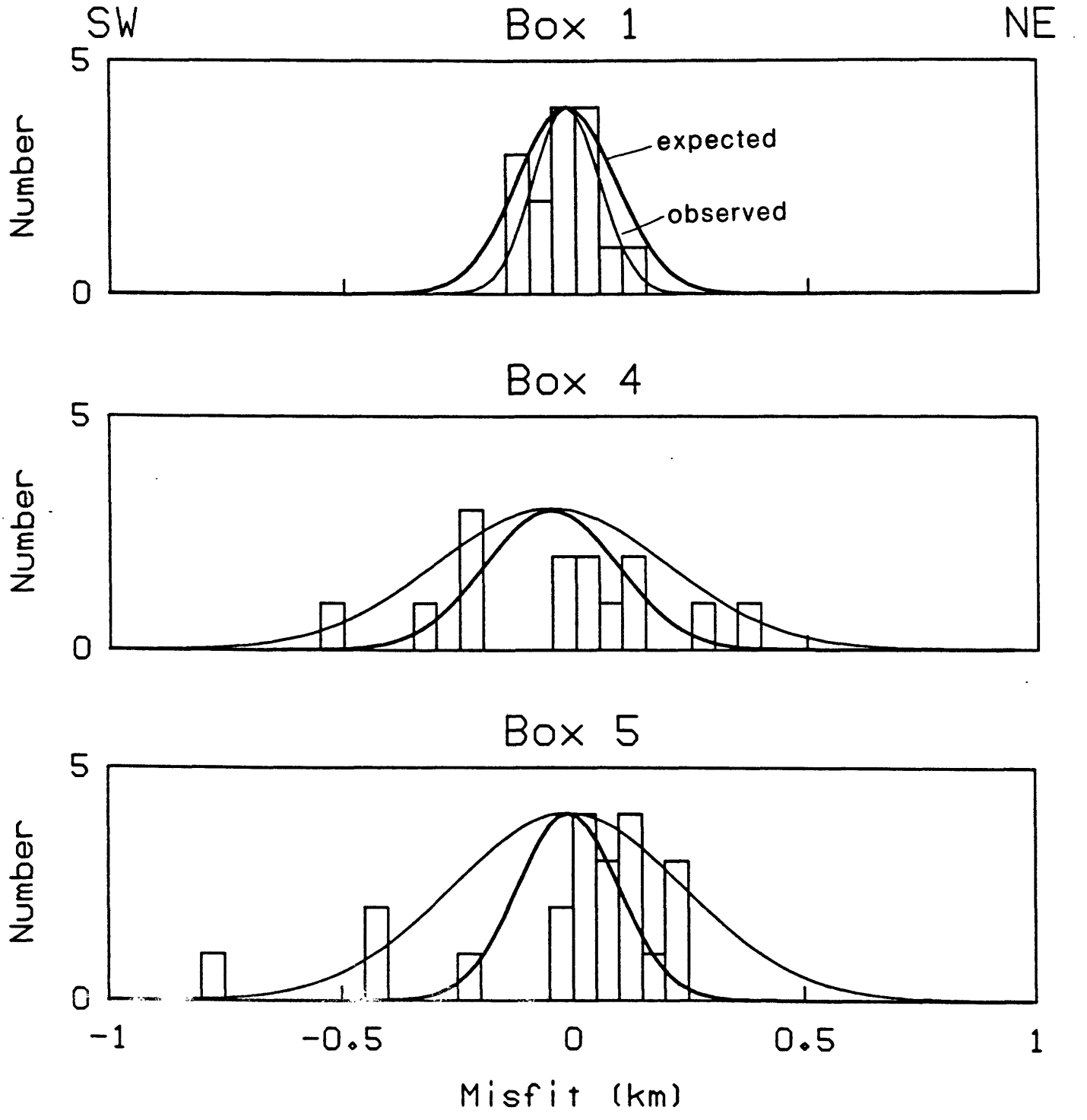
SW
Box 1
NE
5
0
Number
expected
observed
Box 4
5
0
Number
Box 5
5
0
Number
-1
-0.5
0
0.5
1
Misfit (km)

Figure 10

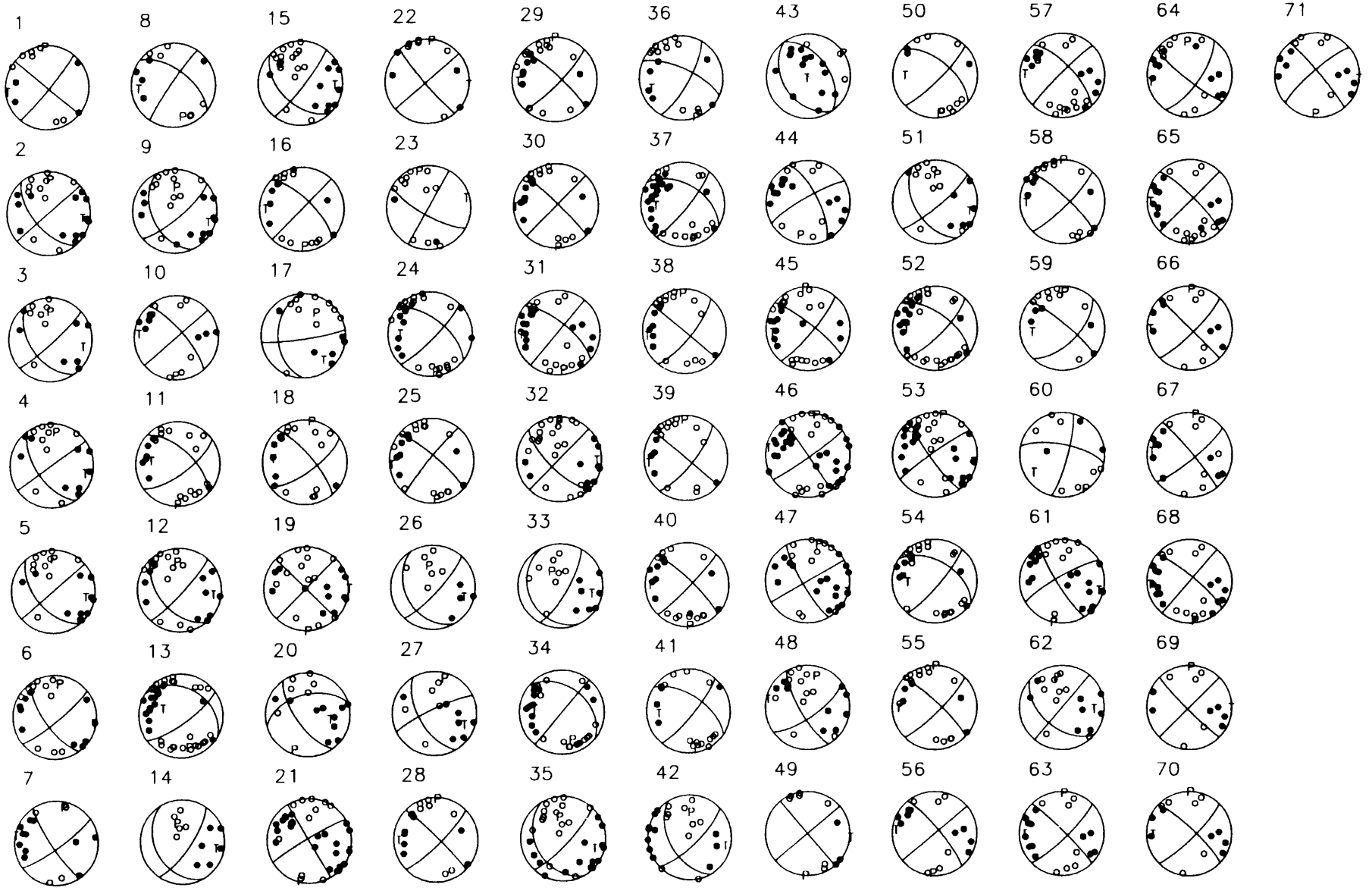
1
8
15
22
29
36
43
50
57
64
71
2
9
16
23
30
37
44
51
58
65
3
10
17
24
31
38
45
52
59
66
4
11
18
25
32
39
46
53
60
67
5
12
19
26
33
40
47
54
61
68
6
13
20
27
34
41
48
55
62
69
7
14
21
28
35
42
49
56
63
70

Figure 11

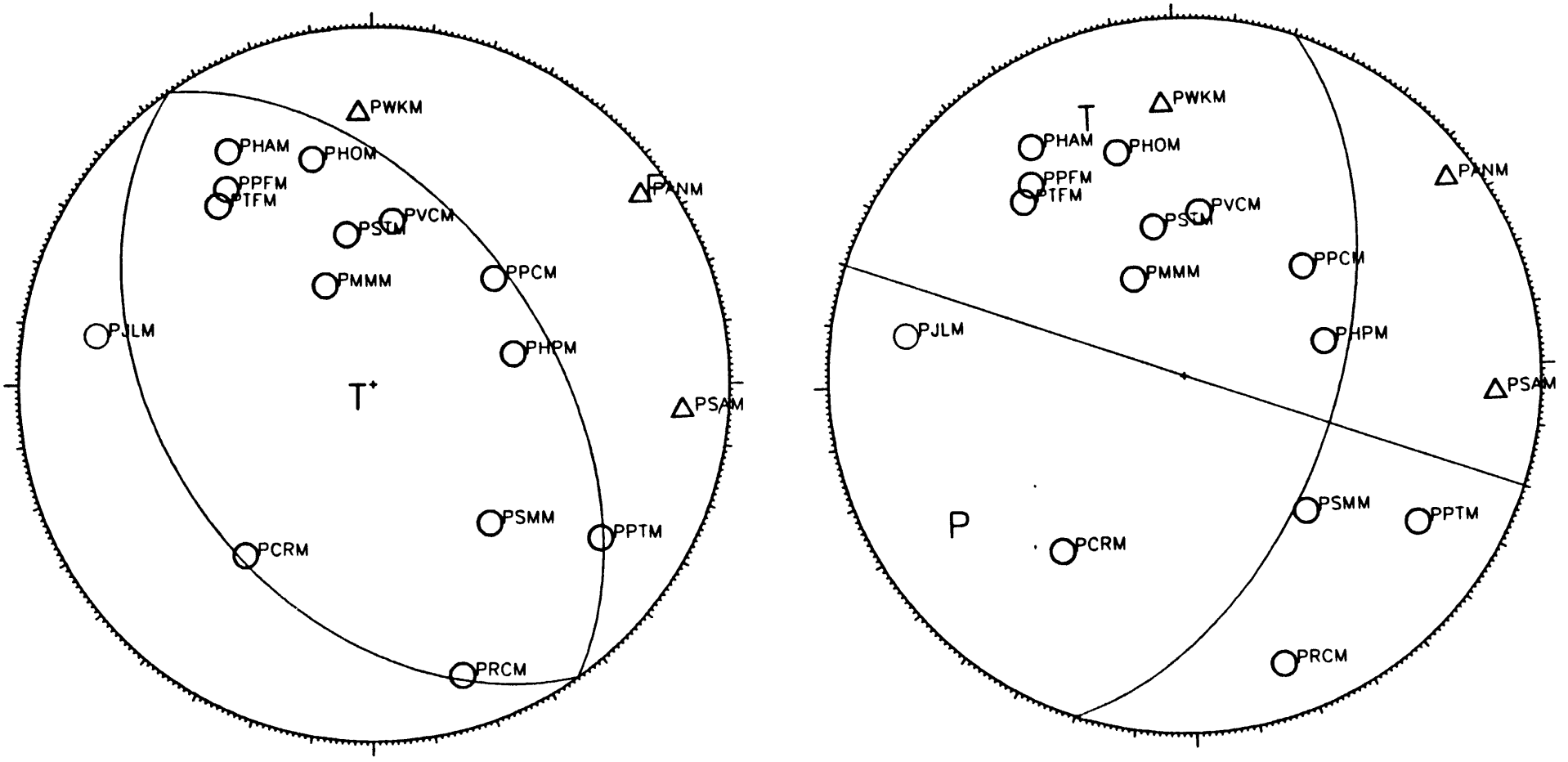

△ DILATATION

○ COMPRESSION

Figure 12

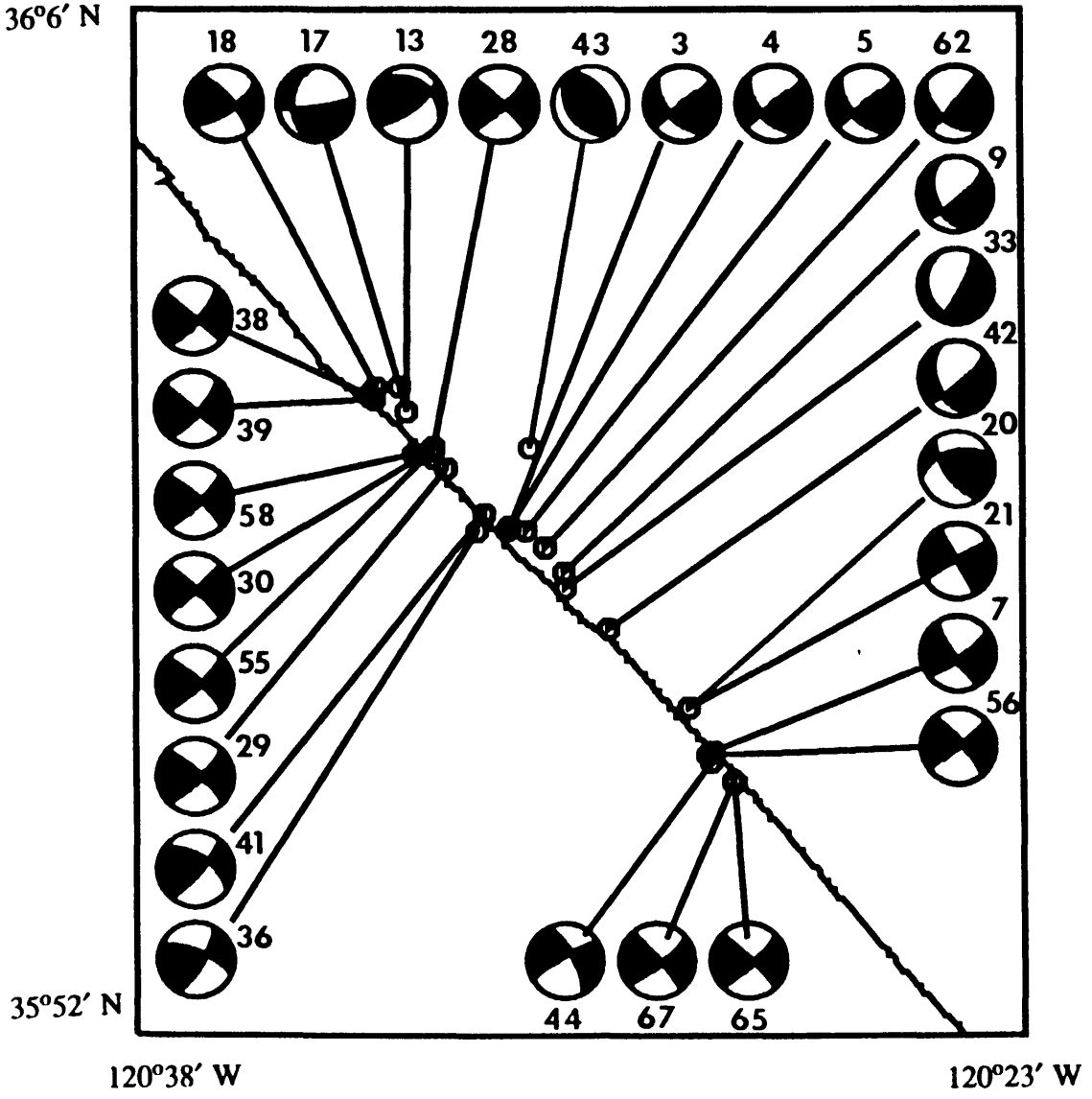
36°6′ N
18
17
13
28
43
3
4
5
62
9
33
42
20
21
7
56
38
39
58
30
55
29
41
36
44
67
65
35°52′ N
120°38′ W
120°23′ W

Figure 13

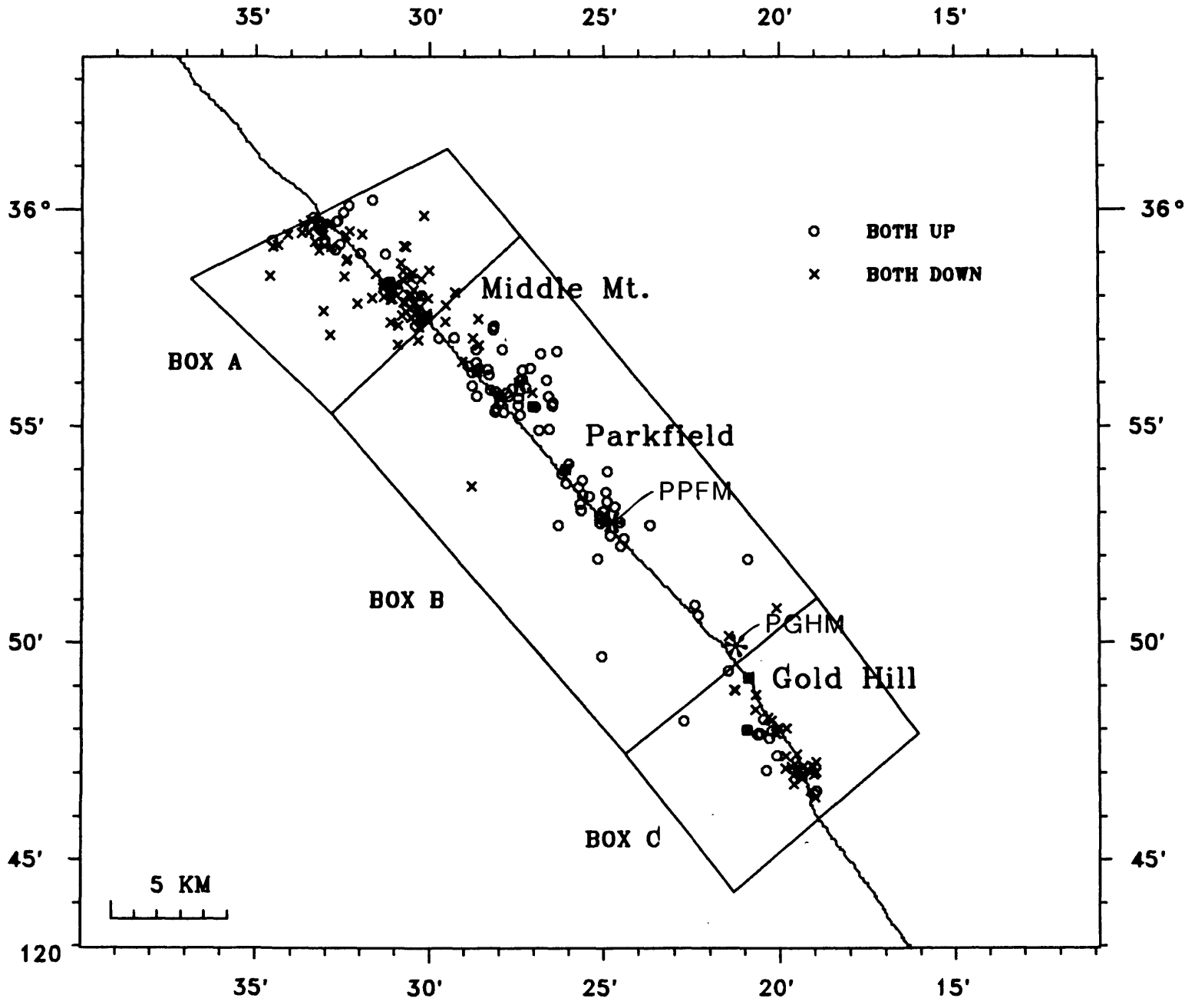
35'
30'
25'
20'
15'
36°
55'
50'
45'
120
BOTH UP
BOTH DOWN
Middle Mt.
Parkfield
Gold Hill
PPFM
PGHM
BOX A
BOX B
BOX C
5 KM

Figure 14